doi:10.1111/j.1365-2591.2008.01454.x

Mechanical behaviour of nickel-titanium rotary endodontic instruments in simulated clinical conditions: a computational study

S. Necchi[1], S. Taschieri[2], L. Petrini[1] & F. Migliavacca[1]

[1]Laboratory of Biological Structure Mechanics, Politecnico di Milano, Milan; and [2]Department of Health Technologies, IRCCS, Galeazzi Institute, Università degli Studi di Milano, Milan, Italy

Abstract

Necchi S, Taschieri S, Petrini L, Migliavacca F. Mechanical behaviour of nickel-titanium rotary endodontic instruments in simulated clinical conditions: a computational study. *International Endodontic Journal*, **41**, 939–949, 2008.

Aim To develop an accurate finite element (FE) model for studying rotary endodontic instruments and to demonstrate the usefulness of the FE method in improving the knowledge of the mechanical behaviour of these instruments during root canal preparation.

Methodology An accurate geometrical model of a Ni-Ti ProTaper F1 instrument was created. The interaction between the rotating instrument and differently shaped root canals during the insertion and removal procedure was studied using FE analyses. The complex thermo-mechanical behaviour of the Ni-Ti alloy was reproduced using an *ad hoc* computational subroutine. With the aim of demonstrating the enhanced performance of the shape memory alloy employment, the same analysis was performed on a 'virtual' ProTaper F1 made of stainless steel.

Results The Ni-Ti instrument operated in its pseudo-elastic range and was able to recover its original shape and to follow the canal curvature without deviation. The radius and the position of the canal curvature are the most critical parameters that determined the stress in the instrument with higher stress levels being produced by decreasing the radius and moving from the apical to the mid root position.

Conclusions The most demanding working conditions were observed in canals with sharp curves, especially in areas where the instruments had larger diameters. To prevent possible damage to instruments and fracture, it is advised that the instruments should be discarded following their use in such canals.

Keywords: finite element method, nickel-titanium alloy, ProTaper, rotary endodontic files.

Received 7 November 2007; accepted 5 June 2008

Introduction

Nickel-titanium engine-driven rotary instruments are used increasingly in endodontic practice (Parashos & Messer 2006). Due to their flexibility, coupled with the design of the blades, it is feasible to use nickel-titanium instruments with a handpiece in a rotary motion to prepare root canals (Sattapan *et al.* 2000). flexibility is conferred by the pseudo-elastic behaviour of the SMA (Shape Memory Alloys, to which the Ni-Ti alloy belongs), i.e. a nonlinear elastic behaviour that allows the material to undergo mechanically induced high deformations without plastic residual strain after stress removal. This behaviour is due to a reversible solid-solid phase transformation between two different crystallographic structures, the austenite and the martensite, which takes place when the working temperature is greater than a value specific one for each alloy (called *austenite finish temperature*, A_f).

The major focus on Ni-Ti instruments has been on the experimental evaluation of their performance

Correspondence: Silvia Necchi, Laboratory of Biological Structure Mechanics, Department of Structural Engineering, Politecnico di Milano, Piazza Leonardo da Vinci, 32 20133 Milano, Italy (Tel.: +39 02 2399 4283; fax: +39 02 2399 4286; e-mail: necchi@stru.polimi.it).

(Hülsmann *et al.* 2005, Taschieri *et al.* 2005) with only two computational studies (as Finite Element Analyses - FEA) being conducted. The main advantage of computational methods is the evaluation of some aspects of the mechanical behaviour of the instruments (e.g. the stress distribution) responsible for their failure, which are difficult to assess through laboratory or *in vivo* tests.

In the FEA performed by Berutti *et al.* (2003), the authors compared the torsional and bending stresses in the geometrical models of two different Ni-Ti instruments. The taper of these instruments was not taken into account. The files were blocked at one end and loaded with a concentrated torsional or bending moment at the opposite end. The nonlinear behaviour of the Ni-Ti was approximated by implementing a stress-strain-curve composed by three linear segments each with a different Young modulus. Results showed that, under equal loading conditions, the ProTaper section model exhibited lower and better distributed stresses than the ProFile section model.

Xu & Zheng (2006) also studied the influence of cross-section profile on the mechanical behaviour of different Ni-Ti instruments by performing FEA. Improving the model proposed in the work by Berutti *et al.* (2003), a constant taper was imposed to the volumes generated by the rotation of the cross-sections. The tip face was constrained and a torque was applied to the free end. A multi-linear kinematic hardening plastic material model was used to approximate the stress-strain relationship of the Ni-Ti alloy. By analysing the results, the authors concluded that: (a) cross-sectional profile had a significant influence on the mechanical behaviour of the instruments and (b) among the models considered, those with convex and triple helix sections were the most torque-resistant.

These two computational studies had limitations. Principally, boundary and loading conditions were dissimilar to that found clinically. At the same time, instrument geometries and constitutive models for the Ni-Ti alloy were not accurate.

The aim of the present study was to create a computational model to simulate the mechanical behaviour of a Ni-Ti rotary endodontic instrument (i.e. ProTaper F1) operating in a root canal. To reach this goal the geometry of the instrument and different root canals were accurately reproduced. Furthermore, an advanced constitutive model for the Ni-Ti alloy was used. The stress that the instrument undergoes during clinical procedures (composed of continuous insertion and removal of the instrument in and out of the canal) was studied to evaluate the effects of the canal shape on the stress state generated in the instrument. A model of a 'virtual' ProTaper F1 made of stainless steel was also considered with the aim of highlighting the advantages derived from the use of Ni-Ti and validate the model in terms of instrument geometry and boundary and interaction conditions.

Materials and methods

The computational analyses were performed using the commercial code ABAQUS 6.5-1/Standard (SIMULIA, Providence, RI, USA). In the following, the FE (Finite Element) model characteristics, in terms of geometry, material, loading and boundary conditions are described.

Geometrical models and meshes

File

A 3D model of the ProTaper finisher file F1 (Dentsply Maillefer Instruments, Ballaigues, Switzerland) was created using the software Rhinoceros 2.0 Evaluation (Robert McNeel & Associates, Seattle, WA, USA).

The file can be divided in three parts: a handle, a smooth shaft and a blade. The handle does not serve any specific function in the shaping procedure, and therefore it was not considered in the analyses.

The proposed model, shown in Fig. 1, accurately reproduced the actual dimensions of the working part of the file, its convex triangular cross-section, the characteristics of the blade, and critical areas of connection between the shaft, the blade and the tip. Particular attention was paid to reproduce the variable taper along the blade of the instrument (Fig. 1c).

The file's 3D geometrical model was meshed using 10-node tetrahedron volumes (Fig. 1d) by means of Gambit 2.2.30 software (Fluent Ansys, Concord, CA, USA). A grid sensitivity study was performed to choose the most convenient number of elements (in terms of computational time and results accuracy), which assured an accurate description of sharp angles and curves.

Canal

Root canal geometry has great variability in terms of diameter and curvature. Pruett *et al.* (1997) suggested a simplified classification of root canals based on their curvature. They indicated the radius and the angle of curvature as discriminating parameters of a canal curvature. The scheme proposed by Pruett *et al.* (1997)

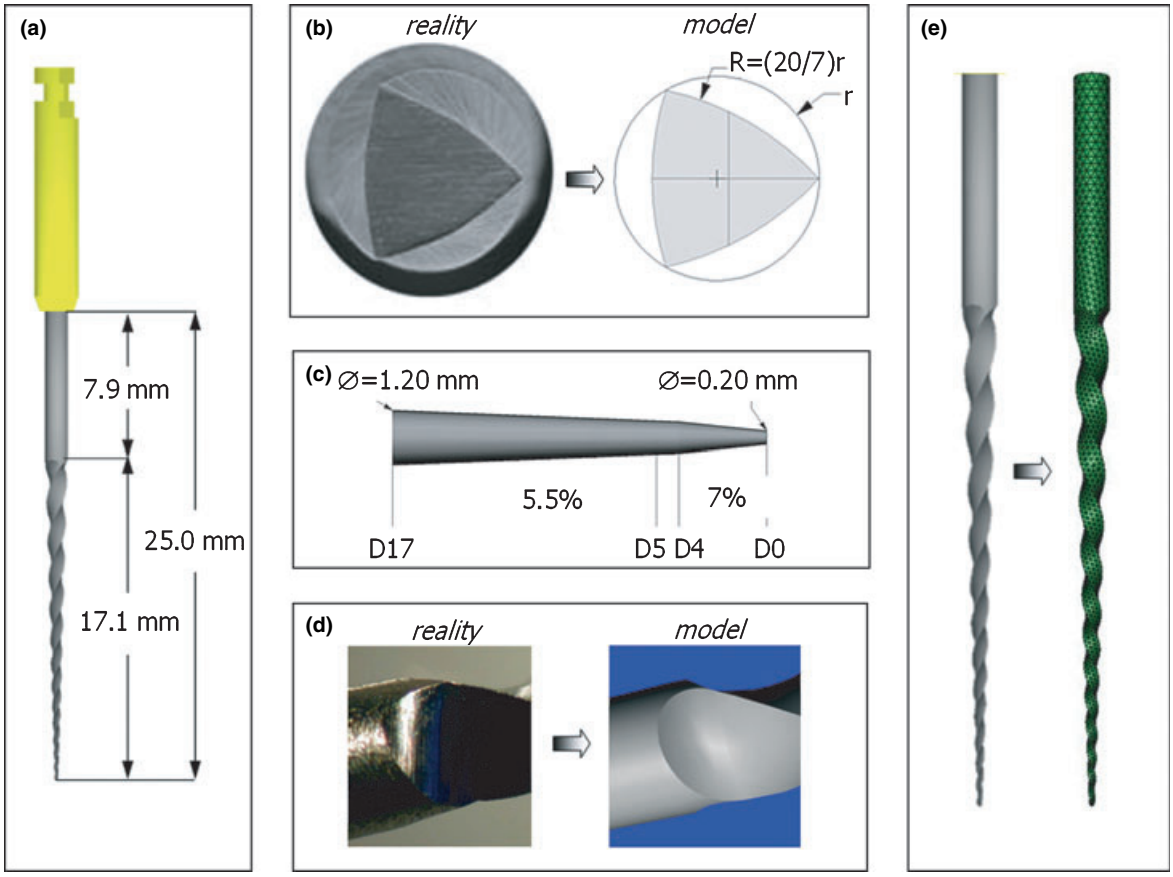

Figure 1 Computational model of the ProTaper finisher instrument F1: 3D geometrical model (a), section (b), blade taper (c), connection part between the shaft and the blade (d), mesh of the working part (e).

was followed in the present study (Fig. 2a), and two values were chosen for both the radius (2 mm, 5 mm) and the angle (30°, 45°) following clinical information. Two positions of the curvature (apical, middle) were also considered, taking into account that the finisher file is used in the final step of the shaping procedure. Therefore, by combining the three cited parameters, seven types (see Table 1) of canal geometries were studied. As examples, see Fig. 2(b,c) for type 3 and type 6.

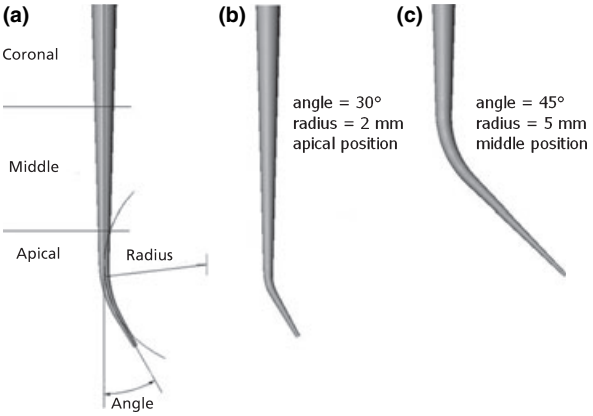

Figure 2 Geometrical model of root canals: characteristic parameters (a), examples of two geometries (b,c).

Table 1 Values imposed on the characteristic parameters of different root canal geometries

Canal type	Curvature angle (degrees)	Curvature radius (mm)	Curvature position
1	30	5	Apical
2	30	5	Middle
3	30	2	Apical
4	30	2	Middle
5	45	5	Apical
6	45	5	Middle
7	45	2	Apical

The canals were modelled as simple rigid surfaces shaped as pipes with a total length of 17 mm according to clinical information. Moreover, the canal diameter was imposed 0.02 mm wider than the file in each file section. In this way, severe and constraining operating conditions were avoided as were possible computational problems due to continuous interaction between instrument and canal.

The 3D models of the canals were meshed directly using the FEA software ABAQUS 6.5–1, using 4-node bilinear elements. A smooth discretization was used to prevent computational problems during the contact between the canal wall and the instrument in the simulations.

Definition of materials

As stated above, two ProTaper finisher file F1 models were considered. First, a Ni-Ti alloy with average properties, described by means of a user-defined subroutine implemented in the ABAQUS code by Auricchio & Petrini (2004). Second, AISI 316L stainless steel, widely used in biomedical applications, described by an elasto-plastic constitutive model with kinematic hardening provided by the computational code library.

In Fig. 3 the uniaxial stress-strain curves of the two models are reported. In both cases, the values of the characteristic parameters (see Table 2) were derived from the literature. Considering the Ni-Ti alloy, the *transformation starting stress* σ_s and the *transformation finishing stress* σ_f, (see Fig. 3), are the stress values at which, at the working temperature, the transformation between austenite and single-variant martensite starts and finishes, respectively. The *limit transformation strain* ϵ_L is the amplitude of the transformation strain interval. The capacity to recover all the deformation (i.e. pseudo-elastic behaviour) finishes when the *martensitic yielding stress* σ_y and the *martensitic yielding strain* ϵ_y (in the following indicated as *pseudo-elastic limits*) are reached. Since the subroutine used is not able to describe the plastic behaviour following yielding of martensite, in this study the simulation results were considered reliable only when stress and strain values were lower than the pseudo-elastic limits. Values of 25 °C and 10 °C were chosen for the working temperature and the temperature A_f, respectively.

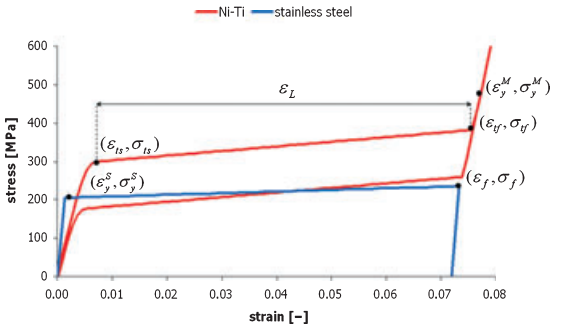

Figure 3 Uniaxial stress-strain curves of the two constitutive materials (Ni-Ti and AISI 316L stainless steel).

Table 2 Values of the characteristic mechanical parameters of the two constitutive models used for describing Ni-Ti and AISI 316L stainless steel in the numerical analyses

Material	Mechanical parameters	Values
AISI 316L stainless steel	Young modulus E [MPa]	193 000
	Poisson ratio ν [-]	0.3
	Yield stress σ_y^S [MPa]	205
	Yield strain ϵ_y^S [%]	0.1
	Fracture stress σ_f [MPa]	515
	Fracture strain ϵ_f [%]	60
Ni-Ti	Young modulus E [MPa]	70 000
	Poisson ratio ν [-]	0.3
	Transformation starting stress σ_{ts} [MPa]	300
	Transformation finishing stress σ_{tf} [MPa]	380
	Limit transformation strain ϵ_L [%]	7
	Martensitic yielding stress σ_y^M [MPa]	480
	Martensitic yielding strain ϵ_y^M [%]	7.7

Boundary and interaction conditions

Clinical operating conditions were simulated by imposing a vertical displacement and a rotation around the longitudinal axis (Fig. 4) on the surface at the interface between the handle and the shaft of the file. In this way, the action of the motor on the instruments was taken into account.

The modelled instruments were moved into the root canals until the apex was reached (i.e. first step of the

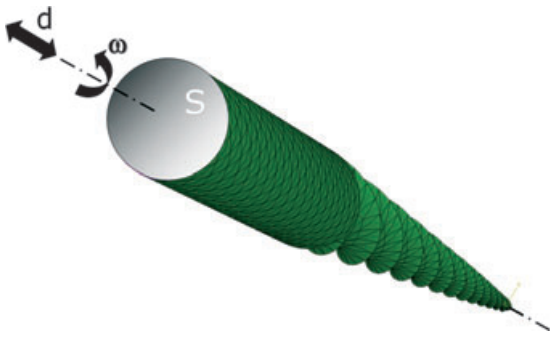

Figure 4 Movements imposed on the instrument: vertical displacement (d) and rotation (ω). S indicates the surface on which the loading and boundary conditions are applied.

procedure, in the following called 'insertion'), and immediately retrieved (i.e. second step of the procedure, in the following called 'removal') in order to prevent blockage.

In clinical use, the instrument rotational speed depends on the motor and the preferences of the clinician. The suggested speed range is 150 to 350 rpm. However, a rotational speed of 25 rpm was employed in this study to avoid excessively long computational time. The results of the analyses were interpreted by considering this simplification.

The interaction between the instrument and the canal was described as a 'soft' contact, exploiting the ABAQUS exponential pressure-overclosure contact model. Moreover, neither friction nor machining action were considered between the blade and the canal wall: hence, the torsional stresses induced in the instrument during the procedure were neglected.

Results

Reference variables

The performance of both the Ni-Ti and stainless steel instruments was studied by analysing the levels of strain during the phases of file insertion and removal into and out of the canals. Indeed, the nonlinear behaviour of both the materials is characterized by high increments of strain but small variations of stress because of the presence of the 'plateau' in their stress-strain curves (see Fig. 3). Therefore the use of the strain as primary variable to compare the mechanical behaviour of both the materials was suggested. In particular, the three-dimensional feature of the analyses led to consider the equivalent strains given by the combination of the strain components in all directions. The obtained scalar values were compared with the limit derived from uniaxial tests.

The strain levels during the simulations were found to be the highest at the end of the insertion step. Therefore, they were analysed mainly in that configuration. The end of the removal step was also analyzed to observe the final conditions of the stainless steel file after a complete insertion-removal cycle; in the case of the Ni-Ti file, at the end of the extraction the original shape (zero stress and strain) was always recovered.

The considered reference variables specific for the Ni-Ti and the stainless steel are provided in Table 3. With regard to the Ni-Ti, if the equivalent transformation strain ϵ_{tr} is lower than the ϵ_L value the recovery of the original undeformed shape is assured once the file is removed from the canal. When ϵ_{tr} reaches the ϵ_L value (transformation end), the shape recovery is still assured if the equivalent total strain ϵ_{tot} does not overcome the pseudo-elastic strain limit ϵ_y.

Table 3 Specific reference variables considered for the evaluation of the deformation of the Ni-Ti and the stainless steel instruments

Material	Reference variable	Meaning
Ni-Ti	ϵ_{tr}, equivalent transformation strain	Instantaneous strain hoarded in the transformation plateau
	ϵ_{tot}, equivalent total strain	Instantaneous total strain the instruments undergoes, sum of the elastic and the transformation component: $\epsilon_{tot} = \epsilon_{el} + \epsilon_{tr}$
Stainless steel	ϵ_{pl}, equivalent plastic strain	Instantaneous permanent deformation that appears whenever the yielding stress σ_y is reached
	ϵ_{tot}, equivalent total strain	Instantaneous total strain the instruments undergoes, sum of the elastic and the plastic component: $\epsilon_{tot} = \epsilon_{el} + \epsilon_{pl}$
	ϵ_{acc}, accumulation of the equivalent plastic strain	Integral of the equivalent plastic strain ϵ_{pl} in a determinate analysis time interval $(0 - \bar{t})$: $\epsilon_{acc} = \int_0^{\bar{t}} \epsilon_{pl} dt$

Influence of curvature parameters

Ni-Ti file

Table 4 provides the values obtained for the equivalent total (ϵ_{tot}) and transformation (ϵ_{tr}) strain at the end of the insertion step. ϵ_{tot} values range between 4.0% and 8.4%, while ϵ_{tr} values range between 3.1% and 7.0%. In particular, the total and transformation strain values are lower than the pseudo-elastic limit only when canals type 1 or type 5 are considered; in all other cases the limit is overcome. The most critical condition is represented by canal type 4 (r = 2 mm, $\alpha = 30°$, position = middle), while the best operating condition is given by canal type 5 (r = 5 mm, $\alpha = 45°$, position = apical).

Table 5 reports the percentages of variation in the strain variables ϵ_{tot} and ϵ_{tr} as functions of the curvature parameters. The radius of curvature seems to be the primary curvature parameter influencing the mechanical behaviour of the instrument. Under the same conditions of angle and position of curvature, higher values of radius produced lower values of strain at the end of the insertion step (Table 5, Fig. 5). In particular, a 5 mm radius generates equivalent transformation strain levels lower than the limit transformation strain: the recovery of the original shape is assured. On the other hand, a 2 mm radius led to critical equivalent transformation and total strain levels in the case of canal 4, while in the case of canals 3 and 7 ϵ_{tr} was limited even if always higher than that of 5 mm radius.

Considering the angle of curvature, an increase of the angle generally implies higher strain values under the same conditions of radius and position of curvature (Table 5), even if very small increments were observed. Only in canals having a curvature in the apical position with a 5 mm radius the change in the angle from 30° (type 1 canal) to 45° (type 5 canal) led to lower values

Table 4 Values obtained for the specific variables concerning the Ni-Ti (total strain ϵ_{tot}, transformation strain ϵ_{tr}) and the stainless steel (total strain ϵ_{tot}, plastic strain ϵ_{pl}) at the end of the insertion step

				Ni-Ti		Stainless steel	
Canal	r	α	Position	ϵ_{tot} (%)	ϵ_{tr} (%)	ϵ_{tot} (%)	ϵ_{pl} (%)
1	5	30	Apical	4.0	3.2	4.6	4.6
2	5	30	Middle	6.6	5.8	7.1	7.1
3	2	30	Apical	7.2	6.4	10.2	10.0
4	2	30	Middle	8.4	7.0	10.9	11.5
5	5	45	Apical	3.9	3.1	4.3	4.2
6	5	45	Middle	6.7	5.9	8.6	8.5
7	2	45	Apical	7.4	6.6	12.1	11.9

Table 5 Percentage of variation in the strain variables reported in Table 3 (ϵ_{tot}, ϵ_{tr}, ϵ_{pl}) as function of the curvature parameters (radius, angle and position) for the Ni–Ti and the stainless steel instruments

				Ni–Ti		Stainless steel	
	Canal	Position	α	ϵ_{tot} (%)	ϵ_{tr} (%)	ϵ_{tot} (%)	ϵ_{pl} (%)
Radius: 2 mm vs. 5 mm	3 vs. 1	Apical	30	+80	+100	+122	+117
	4 vs. 2	Middle	30	+27	+21	+54	+62
	7 vs. 5	Apical	45	+90	+113	+181	+183
			Mean	+66	+78	+119	+121
	Canal	*r*	Position	ϵ_{tot} (%)	ϵ_{tr} (%)	ϵ_{tot} (%)	ϵ_{pl} (%)
Angle: 45° vs. 30°	5 vs. 1	5	Apical	−3	−3	−7	−9
	6 vs. 2	5	Middle	+2	+2	+21	+20
	7 vs. 3	2	Apical	+3	+3	+19	+19
			Mean	+2	+1	+11	+10
	Canal	*r*	α	ϵ_{tot} (%)	ϵ_{tr} (%)	ϵ_{tot} (%)	ϵ_{pl} (%)
Position: middle vs. apical	2 vs. 1	5	30	+65	+81	+54	+54
	4 vs. 3	2	30	+17	+9	+7	+15
	6 vs 5	5	45	+72	+90	+100	+102
			Mean	+52	+60	+54	+57

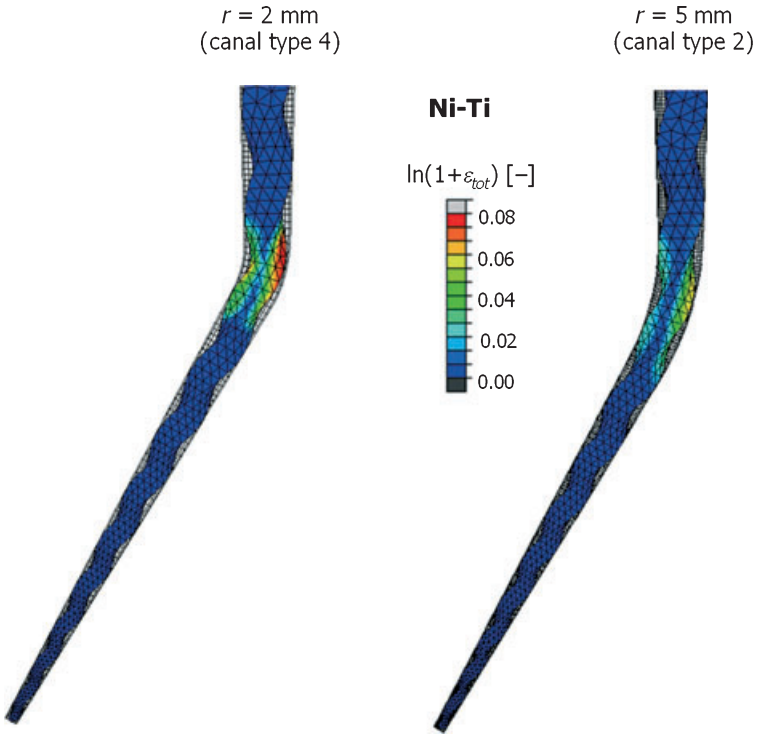

Figure 5 Maps of the maximum total strain in the principal direction resulting at the end of the insertion step of the Ni-Ti instrument in: canal type 4, radius 2 mm (left); canal type 2, radius 5 mm (right).

of strain. Therefore, the angle of curvature does not seem to influence substantially the stress levels.

Considering the position of curvature, shifting from the apical to the middle position results in an increase of the strain values under the same conditions of radius and angle of curvature (Table 5). The rise in the strain level due to a change in the curvature position is lower when canals with a 2 mm radius are considered (canal 3 and canal 4): probably, in these cases the critical radius condition makes the effect of the other curvature parameters negligible. By comparing data in Table 5, the position of curvature along the canal can be judged as the second most influential parameter in the determination of the stress level in the file.

Stainless steel file

Table 4 provides the values obtained for the equivalent total (ϵ_{tot}) and plastic (ϵ_{pl}) strain at the end of the insertion step. The equivalent total strain values varied between 4.3% and 12.1%. In all cases the instrument underwent critical total strain levels, reaching values well beyond the yielding strain (ϵ_y). The values obtained for the stainless steel file were higher in every canal compared to the Ni-Ti instrument. ϵ_{pl} ranged between 4.2% and 11.9% and differently from the Ni-Ti instrument, the most critical condition was represented by canal type 7 (r = 2 mm, α = 45°, position = apical).

As in the case of the Ni-Ti instrument, the radius of curvature was the primary curvature parameter influencing the mechanical behaviour of the instrument (see Table 5). Canal type 5 (r = 5 mm, α = 45°, position = apical) represented the best operating condition independently by the materials adopted. Under the same conditions of angle and position of curvature, greater values of radius produce lower values of strain at the end of the insertion step.

Considering the angle of curvature, analogously to the Ni-Ti instrument, an increase in angle generally (excluding the comparison between canals type 1 and 5) implies higher strain values under the same conditions of radius and position of curvature (Table 5). Even if higher than for the shape memory alloy instrument, also in the stainless steel instrument the increments in the strain values are moderate.

Similar to the Ni-Ti instrument, shifting the curvature from the apical to the middle position resulted in an increase of the strain values under the same conditions of radius and angle of curvature (Table 5). The rise in the strain level was lower when canals with a 2 mm radius were considered.

Table 6 Values of the build up of the plastic deformation (ϵ_{acc}) obtained for the stainless steel at the end of both the insertion and the removal steps

Canal	r	α	Position	Insertion ϵ_{acc} (%)	Removal ϵ_{acc} (%)	Removal vs. insertion ϵ_{acc} (%)
1	5	30	Apical	13.3	17.4	+31
2	5	30	Middle	16.4	18.0	+10
3	2	30	Apical	17.2	20.4	+19
4	2	30	Middle	22.5	30.9	+37
5	5	45	Apical	14.5	20.6	+42
6	5	45	Middle	19.9	22.4	+13
7	2	45	Apical	25.9	34.5	+33

By comparing the stainless steel with respect to the Ni-Ti results, a similar trend in response to a change in the radius, angle and position of curvature can be identified.

The values of the accumulation of equivalent plastic deformation (ϵ_{acc}) obtained for the stainless steel instrument at the end of both the insertion and the removal steps are shown in Table 6. The values vary between 13.3% and 25.9% at the end of the insertion of the instrument into the canal, while the range is between 17.4% and 34.5% at the end of the removal step.

The highest and the lowest values of ϵ_{acc}, considering both the insertion and the extraction steps, were observed in canal type 7 (r = 2 mm, $\alpha = 45°$, position = apical) and type 1 (r = 5 mm, $\alpha = 30°$, position = apical), respectively. As stated above, canal type 7 represents also the most critical conditions in terms of total and plastic strain levels.

As shown in Table 7, when ϵ_{acc} is considered, the influence of the canal geometrical parameters is less evident with respect to the cases discussed previously (Table 5). Nevertheless, the highest influence on the stress levels was always given by the radius of curvature at the end of both the insertion and removal steps (see Fig. 6).

Complying ability of the files

Considering the ability to follow the canal curvature during an entire insertion-removal cycle, the Ni-Ti instrument was able to better conform to the canal shape than the stainless steel instruments (Fig. 7). In particular, the tip of the stainless steel file tended to plasticise just after the first contact with the canals wall. The deformation of the tip determines successive irregular interactions between the file and the wall, and induces the instrument to work in the plastic range of the material for the larger portion of the treatment duration. The Ni-Ti file, instead, bends uniformly along the blade, following the original curvature of the canal. The files demonstrated this behaviour independently of the canal geometry.

Discussion

While investigating instrument behaviour, the essential *in vivo* and *laboratory* studies may be usefully supported by finite element analyses. The numerical simulation of operating conditions, even if described using simplified models, allows quantities not measurable during exper-

Table 7 Percentage of variation in the build up of plastic deformation reported in Table 5 (ϵ_{acc}) as function of the curvature parameters (radius, angle and position) for the stainless steel instruments at the end of the insertion and removal steps

				Insertion	Extraction
	Canal	*r*	α	ϵ_{acc} (%)	ϵ_{acc} (%)
Radius: 2 mm vs. 5 mm	3 vs. 1	Apical	30	+29	+17
	4 vs. 2	Middle	30	+37	+72
	7 vs. 5	Apical	45	+79	+67
			Mean	+48	+52
	canal	*r*	Position	ϵ_{acc} (%)	ϵ_{acc} (%)
Angle: 45° vs. 30°	5 vs. 1	5	Apical	+9	+18
	6 vs. 2	5	Middle	+21	+24
	7 vs. 3	2	Apical	+51	+69
			Mean	+27	+37
	Canal	*r*	α	ϵ_{acc} (%)	ϵ_{acc} (%)
Position: middle vs. apical	2 vs. 1	5	30	+23	+3
	4 vs. 3	2	30	+31	+51
	6 vs. 5	5	45	+37	+9
			Mean	+30	+21

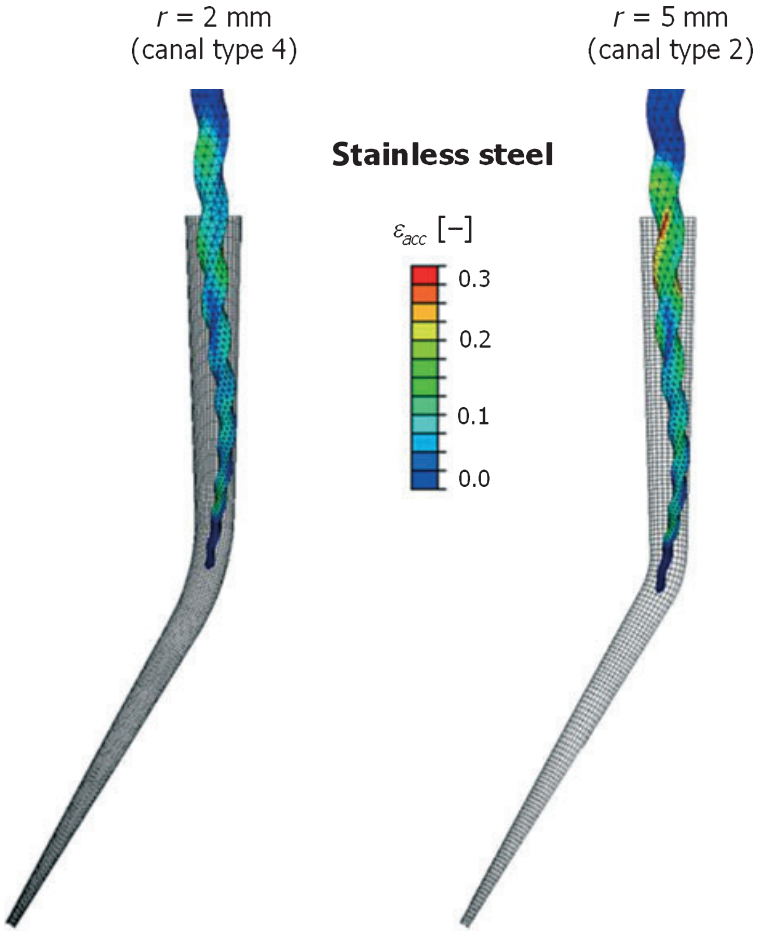

Figure 6 Plastic deformation build up resulting at the end of the removal step of the stainless steel instrument in: canal type 4, radius 2 mm (left); canal type 2, radius 5 mm (right).

iments to be calculated. Moreover, many models (differing in geometry, materials, boundary and loading conditions) may be easily compared. Accordingly, if the limitations and simplifications of the models are accurately recognized, FEA may have an important role in optimizing the behaviour of biomedical devices. From this viewpoint, in this study focus was on the development of a Ni-Ti rotary endodontic instrument (ProTaper finisher file F1) FE model. Geometry, boundary and interaction conditions and material were described accurately. In particular, the multiple taper along the cutting portion of the instrument and the process of insertion and removal of the instrument in curved canals were reproduced. These realistic aspects were not taken into account in previous models (Berutti *et al.* 2003, Xu & Zheng 2006).

The model developed was used to study the influence of canal shape on instrument performance. In particular, flexural stresses varying cyclically during rotation of the endodontic instrument were analysed. The results obtained showed that a decrease in the radius and an increase in the angle imply a rise in the stress and strain levels. These conclusions are in agreement with the outcomes of some laboratory experiments (Pruett *et al.* 1997, Haikel *et al.* 1999, Li *et al.* 2002, Zelada *et al.* 2002, Martín *et al.* 2003, Lopes *et al.* 2007). They confirm that canal geometry influences the tension-compression stresses during insertion-removal cycles, and the fatigue phenomenon as a consequence. Many authors indicate the latter as a primary mechanism responsible for failure (Fife *et al.* 2004, Grande *et al.* 2006, Zinelis *et al.* 2007). On the other hand, in this work torsional stresses induced during instrumentation or generated during critical clinical events such as locking of the file tip into the dentine are not taken into account. This limitation prevent the study of torsional fracture that some authors consider the main cause of instrument failure (Sattapan *et al.* 2000, Yared 2004, Alapati *et al.* 2005, Spanaki-Voreadi *et al.* 2006). Accordingly, a more

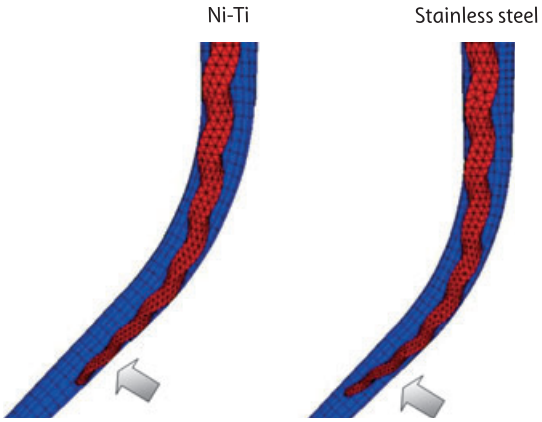

Figure 7 Different ability of the stainless steel (left) and the Ni-Ti (right) instrument to follow the canal shape during the insertion step.

precise FE model, taking into account friction and assessing torsional stress, is currently under development.

In the present research a 'virtual' ProTaper instrument made of stainless steel was also studied, in order to create a computational model with a simpler and better characterized material constitutive model. The analysis of the results allowed a check of the quality of the Ni-Ti model. Moreover, the comparison between the two files confirmed the advantages furnished by the SMA pseudo-elastic behaviour. As expected, the Ni-Ti file showed high flexibility during the transformation of the alloy from austenite to single-variant martensite. This feature allowed the instrument to deform following the canal shape without residual strain, assuring a continuous and regular operation of the instrument. On the contrary, the stainless steel instrument plasticized after the first contact with the canal wall and continued building up plasticity. Critical values of 15%, 20% and even 34% of equivalent permanent deformations were observed in the simulations for different canals. This behavior gives irregular successive interactions with the dentine and might result in abnormal shaping, unpredictable contacts with the canal wall, blockage and even breaking of the file within the canal.

In the implemented Ni-Ti constitutive model the material was assumed to be indefinitely elastic, and the accumulation of plastic deformation due to cyclic loading in the pseudo-elastic ranges was not accounted for. This limitation can cause underestimation of deformation levels. The use of an improved constitutive model should be used in future simulations.

Analogously, assigning a reduced rotational speed to the file is a limitation of the performed simulations. Indeed, a higher number of rotations would have resulted in a higher number of cycles of compression and extension. This restriction affected the results of the simulations with stainless steel, providing low values for the accumulated plastic deformations, while it did not affect SMA simulations because of the omission of the plastic deformation accumulation phenomenon in the material model.

Even under the reported limitations, the analyses allowed the detection of high flexural stress levels that may lead to critical behaviours such as fracture of rotary Ni-Ti instrument. Results demonstrated that a Ni-Ti instrument is able to operate in the desired way, following the canal curvature during penetration and providing an efficient shaping ability. Further useful information could be derived using data on the exact physical and mechanical characteristics of the Ni-Ti alloys used by manufacturers.

The model developed could be used in the future to compare the behaviour of different types of commercially available files and help in the instrument design improvement.

Conclusions

The results of the simulations performed suggest that Ni-Ti behaved as expected and better than stainless steel. Canals with sharp curves, especially in portions that are going to stress the files in their thicker part, represent the most demanding conditions for Ni-Ti instruments in terms of stress and strain conditions. Accordingly, it is advisable to discard instruments used in such canals to prevent their damaged structure causing clinical failures.

Acknowledgements

The authors would like to thank Daniele Aspesi, MEng, for his contribution to the numerical analyses, and Tom Lacey, BSc, for his contribution to the paper drafting. Support from the MIUR (Ministero dell'Istruzione, dell'Università e della Ricerca, Italian Ministry of Education, University and Research) through grant PRIN 2006.

References

Alapati SB, Brantley WA, Svec TA, Powers JM, Nusstein JM, Daehn GS (2005) SEM observations of nickel-titanium

rotary endodontic instruments that fractured during clinical use. *Journal of Endodontics* **31**, 40–3.

Auricchio F, Petrini L (2004) A three-dimensional model describing stress-temperature induced solid phase transformations: solution algorithm and boundary value problems. *International Journal for Numerical Methods in Engineering* **61**, 716–37.

Berutti E, Chiandussi G, Gaviglio I, Ibba A (2003) Comparative analysis of torsional and bending stresses in two mathematical models of nickel-titanium rotary instruments: ProTaper versus ProFile. *Journal of Endodontics* **29**, 15–9.

Fife D, Gambarini G, Britto Lr L (2004) Cyclic fatigue testing of ProTaper NiTi rotary instruments after clinical use. *Oral Surgery, Oral Medicine, Oral Pathology, Oral Radiology, & Endodontics* **97**, 251–6.

Grande NM, Plotino G, Pecci R, Bedini R, Malagnino VA, Somma F (2006) Cyclic fatigue resistance and three-dimensional analysis of instruments from two nickel-titanium rotary systems. *International Endodontic Journal* **39**, 755–63.

Haikel Y, Serfaty R, Bateman G, Senger B, Allemann C (1999) Dynamic and cyclic fatigue of engine-driven rotary nickel-titanium endodontic instruments. *Journal of Endodontics* **25**, 434–40.

Hülsmann M, Peters OA, Dummer PMH (2005) Mechanical preparation of root canals: shaping goals, techniques and means. *Endodontics Topics* **10**, 30–76.

Li UM, Lee BS, Shih CT, Lan WH, Lin CP (2002) Cyclic fatigue of endodontic nickel titanium rotary instruments: static and dynamic tests. *Journal of Endodontics* **28**, 448–51.

Lopes HP, Moreira EJ, Elias CN, de Almeida RA, Neves MS (2007) Cyclic fatigue of ProTaper instruments. *Journal of Endodontics* **33**, 55–7.

Martín B, Zelada G, Varela P *et al.* (2003) Factors influencing the fracture of nickel-titanium rotary instruments. *International Endodontic Journal* **36**, 262–6.

Parashos P, Messer HH (2006) The diffusion of innovation in dentistry: a review using rotary nickel-titanium technology as an example. *Oral Surgery, Oral Medicine, Oral Pathology, Oral Radiology, & Endodontics* **101**, 395–401.

Pruett JP, Clement DJ, Carnes DL (1997) Cyclic fatigue testing of nickel titanium endodontic instruments. *Journal of Endodontics* **23**, 77–85.

Sattapan B, Palamara JE, Messer HH (2000) Torque during canal instrumentation using rotary nickel-titanium files. *Journal of Endodontics* **26**, 156–60.

Spanaki-Voreadi AP, Kerezoudis NP, Zinelis S (2006) Failure mechanism of ProTaper Ni-Ti rotary instruments during clinical use: fractographic analysis. *International Endodontic Journal* **39**, 171–8.

Taschieri S, Necchi S, Rosano G, Del Fabbro M, Weinstein R, Machtou P (2005) Advantages and limits of nickel-titanium instruments for root canal preparation. A review of the current literature. *Schweizer Monatsschrift fur Zahnmedizin* **115**, 1000–5.

Xu X, Zheng Y (2006) Comparative study of torsional and bending properties for six models of nickel-titanium root canal instruments with different cross-sections. *Journal of Endodontics* **32**, 372–5.

Yared G (2004) In vitro study of the torsional properties of new and used ProFile nickel titanium rotary files. *Journal of Endodontics* **30**, 410–2.

Zelada G, Varela P, Martín B, Bahíllo JG, Magán F, Ahn S (2002) The effect of rotational speed and the curvature of root canals on the breakage of rotary endodontic instruments. *Journal of Endodontics* **28**, 540–2.

Zinelis S, Darabara M, Takase T, Ogane K, Papadimitriou GD (2007) The effect of thermal treatment on the resistance of nickel-titanium rotary files in cyclic fatigue. *Oral Surgery, Oral Medicine, Oral Pathology, Oral Radiology, & Endodontics* **103**, 843–7.